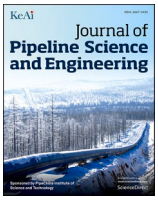
Journal of Pipeline Science and Engineering 6 (2026) 100396

Contents lists available at ScienceDirect

Journal of Pipeline Science and Engineering

journal homepage: www.keaipublishing.com/en/journals/journal-of-pipeline-science-and-engineering/



A numerical study on flow and heat transfer characteristics of the LNG storage tank feed pipeline

Hongyu Zhou, Xu Sun *, Tao Di, Xiaoben Liu, Hong Zhang

National Engineering Research Center for Pipeline Safety/MOE key Laboratory of Petroleum Engineering/Beijing Key Laboratory of Urban Oil and Gas Distribution Technology, China University of Petroleum-Beijing, Beijing 102249, China

ARTICLE INFO

Keywords:
LNG feed pipeline
Numerical simulation
Heat transfer characteristics
Temperature drop rate
Temperature field distribution

ABSRTACT

As a low-carbon fuel, liquefied natural gas (LNG) requires strict temperature control during transportation. Direct injection into pipelines at ambient temperature induces significant thermal stress, potentially causing permanent damage. This study employs numerical simulation to investigate the flow and heat transfer characteristics of LNG feed pipeline during pre-cooling, cold holding, and unloading stages. Significant flow maldistribution and temperature stratification occur during pre-cooling and cold holding, with maximum circumferential and wall-thickness temperature differences reaching 40 K and 23 K, respectively, and a maximum temperature drop rate of 27 K/h. During unloading, the flow reaches full-pipe conditions. While circumferential temperature differences become minimal, the wall-thickness gradient reaches 53 K, with a maximum drop rate of 30 K/min. Cold holding temperature critically affects structural safety, as an excessively rapid temperature drop during unloading may induce thermal stress beyond the material yield limit. To mitigate this risk, a minimum of 23 h of pre-cooling and cold holding is recommended, accompanied by real-time temperature monitoring to ensure thermal stability. Flow rate and fluid temperature are key parameters affecting heat transfer. Inlet temperature exerts a stronger influence on wall temperature than flow rate, suggesting that increasing flow or lowering inlet temperature can improve cooling efficiency. Although unloading rate affects heat transfer, its impact on wall temperature fluctuations is limited. Moreover, complex pipeline structures, such as elbows and T-junctions, induce secondary vortices and flow disturbances, enhancing turbulence and thermal mixing. These effects improve local convective heat transfer and highlight the importance of geometric design in cryogenic pipeline systems.

1. Introduction

Natural gas is widely recognized for its significant advantages as a clean energy source. By 2023, it is projected to account for 26% of global primary energy consumption, with a steady annual increase. The LNG industry has shown significant growth potential. LNG is produced by liquefying natural gas at −162°C, reducing its volume by a factor of 625 (Shukri, 2004). Due to its reduced volume, LNG enhances transportation and storage efficiency, thereby meeting the growing demand for natural gas and becoming a crucial source of imports.

The LNG receiving terminal serves as a crucial transit point for LNG transportation, where natural gas is offloaded from offshore LNG vessels, stored, vaporized, and subsequently delivered to downstream users. Upon arrival at the terminal, LNG is transferred to insulated storage tanks before being transported via gas transmission pipelines. Due to the extremely low temperatures required for LNG transport, and the resulting complex flow behavior, significant temperature fluctuations can induce substantial thermal stresses, potentially compromising pipeline integrity. To prevent thermal stress to the pipelines from the direct inflow of low-temperature LNG, pre-cooling and cold holding operations must be conducted prior to its entry into the pipelines. The pre-cooling process involves the staged injection of low-temperature media, followed by the introduction of boil-off gas (BOG) to establish a cold holding cycle. In the absence of unloading operations, the pipeline remains in this thermally stabilized state. During unloading, a substantial amount of LNG enters the pipeline. Throughout this process, it is crucial to monitor the temperature distribution and variation patterns within the pipeline to ensure its safety. Therefore, it is essential to investigate the temperature dynamics, flow behavior, and associated heat transfer characteristics of the pipeline during the pre-cooling, cold

Peer review under the responsibility of Editorial Board of Journal of Pipeline Science and Engineering.
* Corresponding author.
E-mail address: xsun@cup.edu.cn (X. Sun).

https://doi.org/10.1016/j.jpse.2025.100396
Received 28 February 2025; Received in revised form 24 May 2025; Accepted 26 October 2025
Available online 28 October 2025
2667-1433/© 2025 The Authors. Publishing services by Elsevier B.V. on behalf of KeAi Communications Co. Ltd. This is an open access article under the CC BY license (http://creativecommons.org/licenses/by/4.0/).

holding, and unloading stages.

Many scholars have made significant contributions to the research on pipeline pre-cooling technology. Yuan et al. (2007) conducted pre-cooling experiments on horizontal pipelines using liquid nitrogen and analyzed the flow patterns and heat transfer characteristics. Based on the experimental data, they developed a mathematical model and identified the distinct heat transfer modes at the bottom and top of the pipeline, providing a foundation for a deeper understanding of the heat transfer mechanism. NASA developed the GFSSP software (Liao et al., 2006), which accurately simulates the pre-cooling process of transmission pipelines by considering the effects of flow regimes and component parameters, thereby optimizing pre-cooling duration and liquid nitrogen consumption. Yuan et al. (2009) further explored vertical pipeline pre-cooling through numerical simulations, focusing on the influence of gravity on cooling efficiency. Their results demonstrated that varying flow patterns have a pronounced effect on heat transfer performance. Castillo et al. (2013) analyzed the cyclic performance of compressors and refrigerants during the pre-cooling process at LNG receiving terminals and proposed criteria for thermodynamic evaluation. Johnson et al. (2015) investigated the impact of pipe slope and mass flow rate on cooling efficiency, concluding that an optimized pipe inclination can significantly enhance cooling performance, offering practical insights for pipeline design. Lim et al. (2018) simulated the cooling process under different steady-state flow conditions in vacuum-insulated and polyurethane foam-insulated pipes. The results showed that the polyurethane foam performs better as an insulation material and effectively reduces cooling loss. Jin et al. (2016) conducted experiments on pre-cooling horizontal pipes with liquid nitrogen, used vacuum pipe insulation to reduce heat loss, monitored temperature, pressure, and mass flow during the process. Venkatesh et al. (2023) conducted experimental research on liquid nitrogen pre-cooling and found that bottom heat transfer is less affected by pipe orientation. Li et al. (2024) simulated cooling pipes under different operating conditions and found that the heat transfer surface area is the primary factor affecting cooling rate. Golda et al. (2021) conducted experimental research on cryogenic cooling with liquid nitrogen, proposed the inverse global integration method, and found that surface temperature, nozzle distance, and working pressure of the nitrogen tank are the parameters most influencing heat transfer. Wu et al. (2024) demonstrated that both insulation layer thickness and nitrogen flow rate significantly influence pre-cooling effectiveness, and proposed theoretical formulas for the rapid calculation of pre-cooling temperatures. Zhu et al. (2023) considered pipe size, insulation layer thickness, and material, used a transient mathematical model to optimize the LNG pre-cooling process. Liu et al. (2024) introduced a liquid nitrogen pre-cooling system in the liquefaction process of marine BOG and optimized it by simulation and a bacterial foraging algorithm, significantly reduced unit energy consumption and improved system performance. Soujoudi et al. (2023) evaluated the effect of flash cooling in the pre-cooling cycle through experiments and found it effectively improved the liquefaction process and pre-cooling efficiency. Qyyum et al. (2020) proposed a two-phase expansion technique using a novel binary refrigerant mixture of ethane and nitrogen, significantly improved pre-cooling efficiency. He et al. (2014) experimentally demonstrated that adding a pre-cooling stage effectively reduces the energy consumption of nitrogen pre-cooling. Shaeffer et al. (2013) found that high Reynolds number flows offer more efficient cooling than low Reynolds number or other flow modes. Hu et al. (2012) experimentally studied the cooling process of liquid nitrogen in vertical pipes, compared the cooling rate and flow shape under different flow directions, and analyzed the effect of mass flow on the flow state and heat transfer characteristics.

Many researchers have investigated the flow and heat transfer mechanisms in cryogenic pipelines. Liao et al. (2005) established a quasi-steady-state model to enhance heat transfer in thin film boiling, which can more accurately predict the variation law of the wall temperature of cryogenic fluid in the horizontal pipeline. Zhang et al. (2009) conducted numerical simulations of pre-cooling flow boiling in microchannels and found that the evolution of flow patterns significantly affects heat and mass transfer characteristics. Véchot et al. (2013) experimentally investigated the effects of conduction, convection and radiation on evaporation heat transfer in cryogenic media. Their results indicated that conduction and convection had a far greater impact than radiative heat transfer, and that the liquid level notably affected convective heat transfer intensity. De et al. (2013) studied the flow heat transfer of LNG in finned tubes and determined the relationship between temperature, pressure, velocity, and other parameters with increasing LNG temperature and evaporation. Kuroki et al. (2018) proposed a solution for predicting the pipe wall temperature distribution under unstable cryogenic gas flow at ambient conditions, enabling calculation of the associated heat flux and temperature profiles. Jin et al. (2018) proposed a correlation between the heat transfer of single-phase gas convection and thin film boiling, and applied it to a one-dimensional homogeneous transient heat transfer model, which can accurately predict the cooling time of tubes and the consumption of liquid nitrogen within a certain mass flow range. Liu et al. (2024) developed a new delta airfoil eddy current generator, which can significantly improve the heat transfer efficiency of heat exchangers. Wang et al. (2023) experimentally found that increasing the LNG mass flow rate improved the two-phase flow distribution, thereby improving the heat transfer efficiency. Kunniyoor et al. (2021) developed a predictive model for liquid nitrogen pipelines that considered the interaction between heat transfer and pressure drop. Darr et al. (2020) established a numerical model of two-phase flow convection heat transfer in liquid hydrogen pipelines, which could more accurately predict the cooling time of liquid hydrogen pipelines and the changes in pipeline temperatures.

The literature review reveals that current research on cryogenic fluid flow primarily focuses on simple pipeline structures, such as straight or curved pipes, while in-depth studies on the flow and heat transfer characteristics of cryogenic media in complex pipeline systems are lacking. Additionally, studies on the feed pipelines of LNG receiving terminals mainly focus on the pre-cooling process, with no comprehensive research available on the entire workflow, including pre-cooling, cold holding, and unloading. As shown in Fig. 1, an LNG receiving terminal discovered four crack defects at the weld joints between the valve sleeves of the upper inlet pipe. These defects include one transverse crack and three longitudinal cracks, all located on the valve side of the weld. The formation mechanisms of these cracks are still unclear. Given the current lack of understanding regarding the flow characteristics and temperature distribution in LNG feed pipelines, conducting relevant research is crucial for revealing the temperature variation patterns and flow states, and holds significant theoretical and engineering value.

This study employs numerical simulation to investigate the flow and heat transfer characteristics of the LNG feed pipeline under operational conditions. Firstly, a three-dimensional model of the LNG feed pipeline is developed. Secondly, the Reynolds-Averaged Navier–Stokes (RANS) method is employed to simulate the flow characteristics and

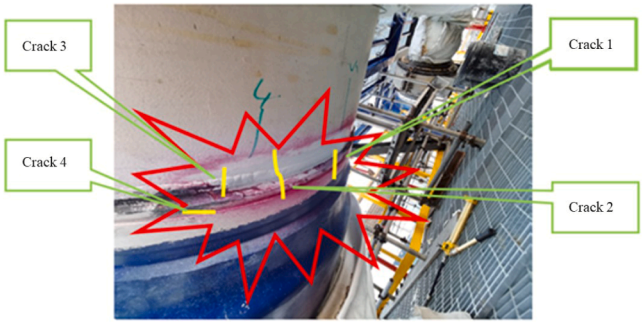


Fig. 1. Cracks in the feed pipeline at an LNG receiving terminal.

temperature distribution of the LNG feed pipeline, and its accuracy and stability are validated with benchmark models. Finally, the heat transfer characteristics and their evolution under various operating conditions are comprehensively analyzed, with a particular focus on elucidating the underlying heat transfer mechanisms of the LNG feed pipeline under different operating conditions. Furthermore, the dominant factors affecting heat transfer efficiency are systematically identified. The results fill the theoretical gap in the study of LNG pipeline operations, providing a solid theoretical foundation and practical guidance for the safe and efficient operation of the LNG receiving terminals.

2. Governing Equations

The heat transfer mechanism in LNG feed pipelines is complex, as it is influenced by both convection and conduction, which are closely related to the fluid flow state. Heat transfer among the feed pipeline, the fluid, and the external environment primarily involves the following aspects: (1) Heat conduction: The conduction process occurs between the pipe wall and the insulation layer, with heat transferred from the warmer insulation layer to the pipe wall. (2) Convection: Forced convection occurs between the fluid and the inner pipe wall, while natural convection takes place between the outer surface of the insulation layer and the surrounding environment. The Nusselt number is usually employed to characterize the strength of convection heat transfer, as expressed in Eq. (1).

$$Nu = \frac{h \cdot l}{k} \tag{1}$$

where h is the area-averaged convective heat transfer coefficient over the pipe wall surface; l is the geometric characteristic length of the heat transfer surface (the inner diameter of the pipe); k is the thermal conductivity of the fluid.

During the solution process, the developed numerical model must satisfy the continuity, momentum, and energy equations (Eqs. (2)-(4)). The selection of an appropriate turbulence model depends on fluid properties and specific numerical requirements. Common turbulence models include the Spalart-Allmaras SA model, the k-epsilon model, the k-omega model, the DES model, and the LES model. In this study, the k-epsilon model is selected based on its widespread use in engineering and its ability to provide stable and accurate results. This selection is informed by a detailed description of the engineering problem related to the LNG feed pipeline. The k-ε model is further subdivided into three versions: the standard k-ε model, the RNG k-ε model, which accounts for the effects of vortices, and the realizable k-ε model, which introduces a change in the viscosity of molecules to simulate a variety of complex flow environments. The realizable k-ε model is selected due to the complexity of the LNG feed pipeline model and the numerous changes in the flow path inside the pipeline. The model consists of two transport equations, as shown in Eqs. (5) and (6).

$$\frac{\partial \rho}{\partial t} + \frac{\partial (\rho u)}{\partial x} + \frac{\partial (\rho v)}{\partial y} + \frac{\partial (\rho w)}{\partial z} = 0 \tag{2}$$

$$\rho \frac{\partial u_i}{\partial t} + \rho u_j \frac{\partial u_i}{\partial x_j} = -\frac{\partial p}{\partial x_i} + \frac{\partial \tau_{ij}}{\partial x_j} + F_i + \rho g_i \tag{3}$$

$$\rho C_p \frac{\partial T}{\partial t} + \rho C_p u \cdot \nabla T = \beta T \left(\frac{\partial p}{\partial t} + u \cdot \nabla p \right) + \tau : S + \nabla \cdot (\lambda \nabla T) + H \tag{4}$$

$$\frac{\partial (\rho k)}{\partial t} + \frac{\partial (\rho k u_j)}{\partial x_j} = \frac{\partial}{\partial x_j} \left[\left(\mu + \frac{\mu_t}{\sigma_k} \right) \frac{\partial k}{\partial x_j} \right] + G_k + G_b - \rho \varepsilon - Y_M + S_k \tag{5}$$

$$\begin{aligned} \frac{\partial (\rho \varepsilon)}{\partial t} + \frac{\partial (\rho \varepsilon u_j)}{\partial x_j} &= \frac{\partial}{\partial x_j} \left[\left(\mu + \frac{\mu_t}{\sigma_\varepsilon} \right) \frac{\partial \varepsilon}{\partial x_j} \right] + C_{1\varepsilon} \frac{\varepsilon}{k} (G_k + C_{3\varepsilon} G_b) \\ &\quad - C_{2\varepsilon} \rho \frac{\varepsilon^2}{k} + S_\varepsilon \end{aligned} \tag{6}$$

where ρ is the density of the fluid; t is time; x, y, z is the coordinates of the mass in space; u, v, w is the velocity component of the mass velocity; p is the pressure on the fluid mass; τ_{ij} is the molecular viscous stress; F_i denotes the volumetric force; g_i denotes the gravitational volumetric force; T is the temperature; C_p is the constant-pressure specific heat; β is the volume expansion coefficient; τ is the viscous stress tensor; S is the strain rate tensor; λ is the thermal conductivity; H is the volume source term; μ_t is the turbulent eddy viscosity, taken as a constant 0.09; k is the turbulent kinetic energy; ε is the dissipation rate; μ is the kinetic viscosity; G_k is the turbulent kinetic energy due to the mean velocity gradient; G_b is the turbulent kinetic energy due to the effects of buoyancy; $C_{1\varepsilon}$, $C_{2\varepsilon}$, $C_{3\varepsilon}$ is an empirical constant, generally taken as $C_{1\varepsilon} = 1.44$, $C_{2\varepsilon} = 1.92$, $C_{3\varepsilon} = 0.09$; σ_k, σ_ε are the Prandtl numbers corresponding to the turbulent kinetic energy and turbulent dissipation rate, respectively, generally taken as $\sigma_k = 1.0$, $\sigma_\varepsilon = 1.3$; Y_M is the contribution of fluctuating expansion to the total dissipation rate in compressible turbulence; S_k, S_ε is the source item.

Eqs. (2)-(6) are solved by ANSYS Fluent 22.0 software, using finite volume method. The turbulence model is the realizable k-ε model; the wall function is scalable wall function; the pressure-velocity coupling is coupled; the spatial discretization of gradient is least squares cell-based; the spatial discretization of pressure is second order; the spatial discretization of momentum is second-order upwind; the spatial discretization of energy is second-order upwind; the transient formulation is bounded second order implicit; the residuals of *x, y, z* velocity components and continuity are taken as the convergence monitors. The convergence criteria for continuity is 10^{-6} and the others are all 10^{-5}.

The operation of an LNG feed pipeline involves numerous procedures and field treatments. To facilitate the numerical simulation, the following assumptions are made for the model:

(1) The physical properties of the pipeline and the insulation material are assumed to remain constant despite temperature variations;

(2) The cold loss generated during the operational process is disregarded;

(3) During the unloading process, LNG is in a full-flow state, and phase change is neglected under ideal conditions.

3. Numerical Method and Validation

To ensure the accuracy of the simulation method, a model is developed using actual operational data from an LNG receiving station in Hainan, China. The calculation method for the LNG feed pipeline is validated by comparing simulation results with field monitoring data.

3.1. Validation of the calculation method

To verify the accuracy of the numerical model, verification calculations were performed using actual operational data from an LNG receiving station in Hainan, China. The simulation results were compared with the station's monitoring data for validation. Based on the parameters in Table 1, a 100-meter horizontal pipeline model was established, with boundary conditions matching the actual pre-cooling conditions. The operating parameters were shown in Table 2, and the external ambient temperature was set to 303 K. Fluent software was used to apply the RANS method for solving the turbulence model. The model was set to Realizable k-ε, with the boundary layer treatment extended using the wall function. The energy equation was enabled, and the process accounted for the effects of gravity and buoyancy. The pipeline cooling layer was modeled with natural convective heat transfer, while the remaining contact surfaces were modeled with

Table 1
Parameters of pipeline.

Parameters	Material	Size (mm)	Thermal conductivity (W/(m·K))	Specific heat capacity (J/(kg·K))	Density (kg/m^3)
Pipe	stainless steel	1,016	16.3	500	7,930
Inner cooling layer	PIR	160	0.02	1,380	50
Outer cooling layer	foam glass	70	0.062	688.9	160

Table 2
Pre-cooling boundary conditions.

Pre-cooling stage	Inlet temperature (K)	Inlet mass flow rate (kg/s)	Pressure (MPa)	Time (h)
1	263	0.83	0.1	3.5
2	243	0.83	0.1	1.5
3	228	0.83	0.1	2
4	213	0.83	0.1	2

coupled heat transfer.

The model mesh is shown in Fig. 2, a structured mesh was employed for the straight pipe section due to its regular geometry. To accurately capture near-wall flow behavior, an inflation layer was applied along the fluid boundary. The boundary layer mesh consists of 9 layers, with the first layer thickness set to 0.1 mm and a growth rate of 1.1 to ensure sufficient resolution of the velocity and thermal gradients near the wall. The overall mesh quality was maintained above 0.7, supporting numerical stability and solution accuracy throughout the domain. The temperature monitoring points were placed 50 meters from the pipeline entrance, at the top and bottom of the pipe, corresponding to the locations of the on-site monitoring points. A comparison was made between the numerical simulation results and the field data, and the calculation results and errors are presented in Table 3.

Comparison of the simulation results with field data indicated that the simulated temperature at the bottom of the pipe was in close agreement with the actual data, exhibiting a maximum error of 3.5 K and a relative error of 1.25%. At the top of the pipe, the simulated temperature showed a deviation from the measured value, with a maximum error of 7.6 K and a relative error of 2.80%. The overall decreasing trend in pre-cooling temperature along the pipeline was consistent with experimental observations, with a maximum deviation below 3%, thereby confirming the reliability of the simulation methodology.

3.2. Grid-independence test

Due to the geometric complexity of the pipeline, an unstructured mesh was adopted. To accurately capture the fluid flow within the pipe, the mesh was refined in the fluid domain, and additional boundary layer grids were applied near the pipe wall. The boundary layer consisted of nine layers, with the first layer thickness set to 0.1 mm and a growth rate of 1.1, ensuring sufficient resolution for high-accuracy simulation. To verify the mesh independence, four models with different mesh numbers were constructed, and the detailed mesh parameters are listed in Table 4. Additionally, Fig. 3 illustrates the grid layout of these four models in the upper inlet pipe region.

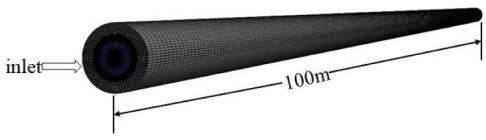


Fig. 2. Computational mesh of the pipeline.

As illustrated in Fig. 4, the temperature results at the monitoring point are presented for different mesh models under identical working conditions. Mesh 1 has fewer elements, causing its results to deviate from those of the other three models. When the simulation time ranges from 1 to 2 hours, deviations were still observed between the results at temperature monitoring points for mesh 2 and those for meshes 3 and 4. In contrast, meshes 3 and 4 yielded consistent results overall. Meshes 1 and 2 exhibited significantly lower quality than meshes 3 and 4, while mesh 4 entailed a much higher computational cost. Considering mesh quality, simulation accuracy, and computational efficiency, mesh 3 was selected for subsequent simulations.

3.3. Time-step independence test

To ensure the accuracy of the results, it is essential to verify that the time step does not significantly influence the simulation results. Mesh 3 was employed under constant conditions, with time steps of 1, 2, 3, and 5 seconds applied in the simulations. It is important to note that the selection of time step plays a crucial role in both the accuracy and numerical stability of the simulation. An excessively large time step can not only reduce the precision of the results but also hinder the convergence of the numerical solution, particularly under complex conditions involving strong nonlinearity and rapid physical changes. Therefore, selecting an appropriate time step is critical to ensuring both reliable results and a stable computation process.

As shown in Fig. 5, within the first 1.5 hours of the pre-cooling stage, the simulation results for time steps of 3 and 5 seconds deviated from those using time steps of 1 and 2 seconds. Furthermore, the complexity of the fluid flow within the pipe must be considered. Specifically, the pre-cooling and cold holding stages involved the staged introduction of fluids with varying inlet temperatures, resulting in a highly unsteady thermal field. To better capture these gradual changes while balancing computational cost, a time step of 2 seconds was selected for these stages.In contrast, during the unloading process, the fluid exhibited a high flow rate and ultra-low temperature, leading to the temperature field to change more abruptly. To accurately capture these rapid variations and maintain numerical stability, a finer time step of 1 second was employed.

4. Results and Discussions

4.1. Computational model

Fig. 6(a) is the 2# storage tank in LNG receiving station, and the feed pipeline of the 2# storage tank is selected for analysis, as shown in Fig. 6 (b). The pipeline model was developed based on field data, divided into four sections: the pipe in front of the tank, the riser, the upper inlet pipe, and the lower inlet pipe. The valves in the pipeline have minimal impact on the calculation results and are simplified as segments of equal length in the model. The pipeline is 75 meters long, with one inlet and two outlets (labeled as upper outlet 1 and lower outlet 2), a diameter of 1016 mm, a wall thickness of 13.2 mm, and a cold-retaining layer thickness of 300 mm. As shown in Fig. 6(c), pre-cooling is performed by passing low-temperature nitrogen, and liquid nitrogen is injected into the pipeline on the platform in front of the tank via a temporary pipeline after being gasified in the carburetor by the tanker truck. It flows through the risers along the feed pipeline to the upper and lower inlet valve groups, and finally enters the storage tank. During unloading, after the LNG ship docks at the quay, the output pipeline on the carrier is connected to the station's unloading pipeline via the unloading arm, and LNG is transferred to 2# tank through the pre-cooled feed pipeline using the on-board transfer pump. Based on the density of LNG in the transport vessel and the storage tank, it is determined whether to use the up-

Table 3
Comparison of simulation results with actual monitoring results.

Time (h)	Top temperature (K)				Bottom temperature (K)			
	Simulated value	Actual value	Absolute error	Relative error	Simulated value	Actual value	Absolute error	Relative error
0	303	304.1	−1.1	0.36%	303	302.7	0.3	0.09%
1.5	301.15	302.6	−1.45	0.47%	289.78	288.1	1.68	0.58%
2	300.32	301.7	−1.38	0.45%	285.5	282	3.5	1.24%
2.5	299.46	300.2	−0.74	0.24%	281.84	279	2.84	1.02%
3	298.5	298.7	−0.2	0.06%	278.52	277.5	1.02	0.36%
3.5	297.47	297	0.47	0.15%	275.97	274.9	1.07	0.38%
4	296.25	295	1.25	0.42%	272.03	270	2.03	0.75%
4.5	294.92	292.6	2.32	0.79%	268.01	264.7	3.31	1.25%
5	293.44	290.1	3.34	1.15%	263.92	261	2.92	1.12%
5.5	291.84	287	4.84	1.68%	258.69	256	2.69	1.05%
6	290.13	284.5	5.63	1.97%	254.14	252.2	1.94	0.77%
6.5	288.3	281.4	6.9	2.45%	250.11	247.9	2.21	0.89%
7	286.36	278.7	7.66	2.74%	246.75	245	1.75	0.71%
7.5	283.27	276.1	7.17	2.59%	243.56	243.1	0.46	0.19%
8	281.05	273.6	7.45	2.72%	240.53	240.3	0.23	0.09%
8.5	278.7	271.1	7.6	2.80%	237.49	237	0.49	0.21%
9	276.17	268.6	7.57	2.81%	234.25	232.9	1.35	0.57%

Table 4
Parameters for different grids.

Mesh	Number of grid elements	Minimum orthogonal mass	Maximum aspect ratio
Mesh1	988,822	0.31	59.63
Mesh2	1805,170	0.38	42.31
Mesh3	3666,738	0.50	30.47
Mesh4	6741,210	0.52	33.61

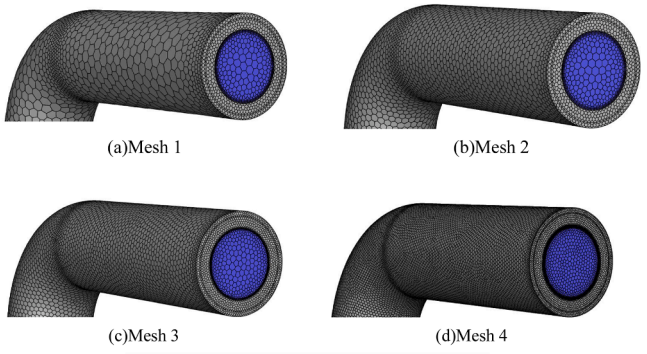


Fig. 3. Model with different number of grid elements.

feeding or down-feeding method: if the LNG density in the vessel is higher than that in the storage tank, the up-feeding valve opens; if the LNG density in the vessel is lower, the down-feeding valve opens.

The simulation boundary conditions are defined based on the field operating conditions. The pipeline pre-cooling is divided into six stages, while cold holding is carried out in a single stage. During the unloading process, due to cracks identified in the up-inlet pipeline, necessitating the use of up-inlet pipeline parameters as boundary conditions. Nitrogen is used in the pre-cooling stage, converting to BOG when entering the cold holding, while LNG serves as the medium in the unloading stage. The unloading stage, characterized by ultra-low temperature and high flow rate, exhibits a temperature field that stabilizes more quickly. Therefore, the simulation results from the first two hours are selected for analysis, with the boundary conditions outlined in Table 5.

The LNG is transported by sea, containing primarily methane and no impurities. The numerical simulation results using methane properties closely match those obtained with LNG properties. Therefore, methane is used as a substitute for LNG in this simulation. The cold-retaining layer boundary is modeled with natural convective heat transfer to the

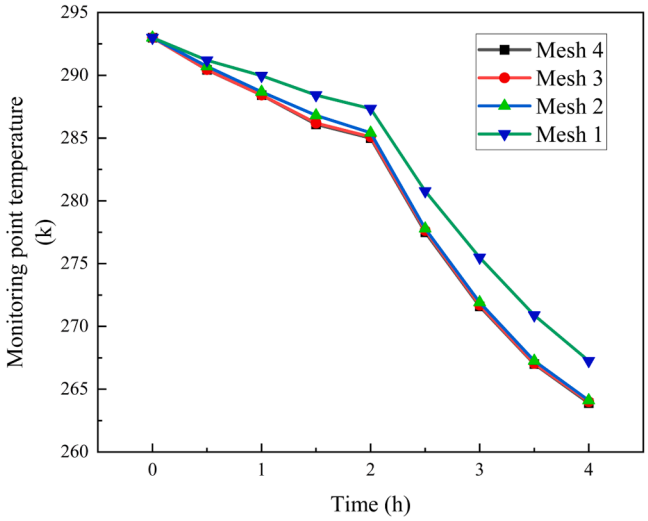


Fig. 4. Comparison of temperature at monitoring points with different grid models.

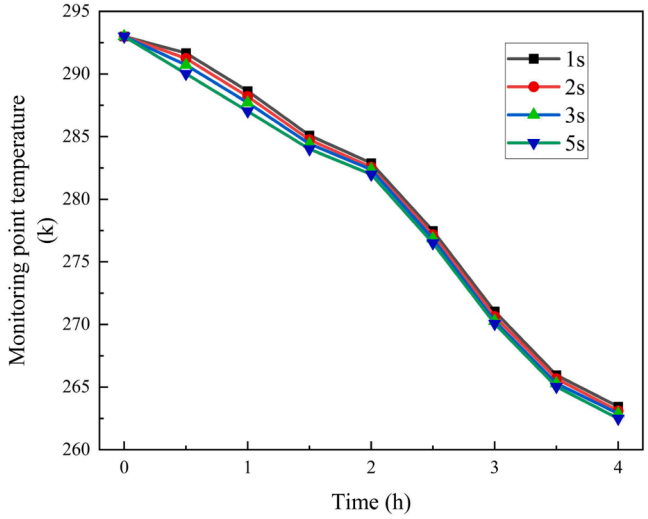
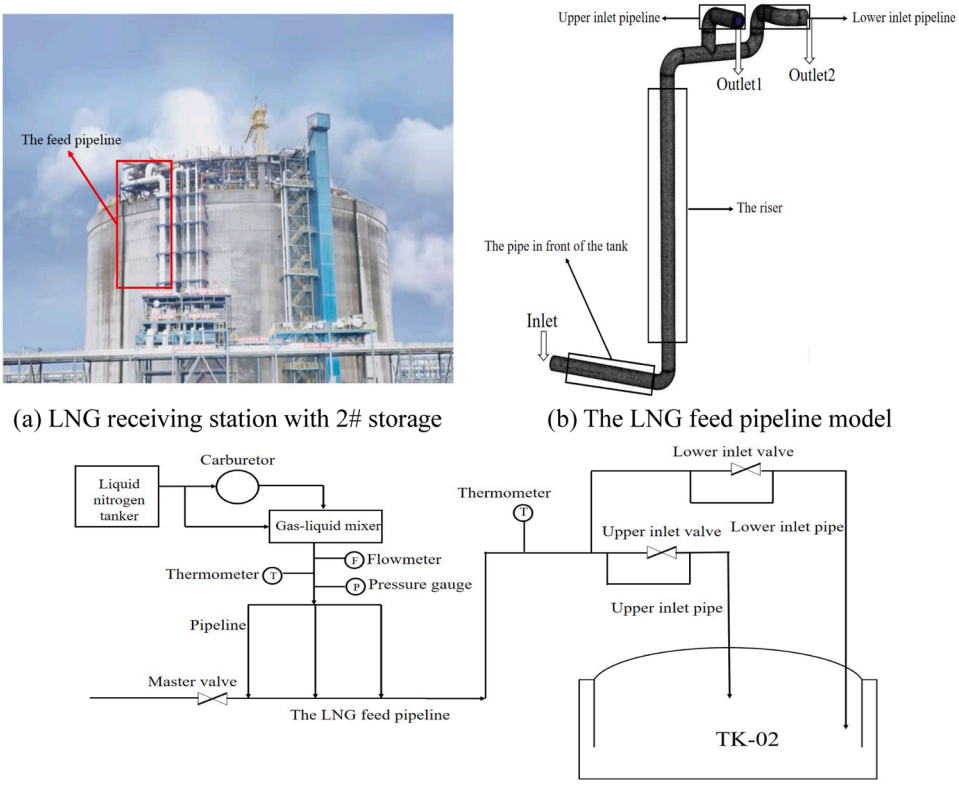


Fig. 5. Comparison of monitoring point temperatures at different time steps.



(a) LNG receiving station with 2# storage

(b) The LNG feed pipeline model

(c) The LNG Receiving terminal process flow

Fig. 6. LNG receiving terminal.

Table 5
Boundary conditions.

Condition	Inlet temperature (K)	Inlet pressure (MPa)	Inlet flow rate (m/s)	Time (h)
Pre-cooling Stage 1	273	0.15	0.1	2
Pre-cooling Stage 2	243	0.15	0.215	2
Pre-cooling Stage 3	243	0.15	0.36	1
Pre-cooling Stage 4	213	0.15	0.36	3.5
Pre-cooling Stage 5	183	0.15	0.36	2.5
Pre-cooling Stage 6	130	0.15	0.36	6
Cold holding stage	125	0.156	0.06	6
Unloading stage	115	0.158	4.5	2

atmosphere, with a heat transfer coefficient of 8.141 W/(m^2·K) and an external ambient temperature of 293 K. The initial temperature of the pipeline is set to 293 K. As shown in Fig. 7, 29 temperature monitoring sections are established along the LNG feed pipe to ensure comprehensive coverage of temperature variations across different segments. At each section, eight temperature monitoring points are evenly positioned around the pipe wall circumference. Sections 28 and 29 are specifically located at the upper feed pipe where cracks have been observed, temperature monitoring points are placed in both the fluid and solid domains of the upper inlet pipe to thoroughly analyze the temperature variation in the cracked region.

4.2. Pre-cooling and cold holding

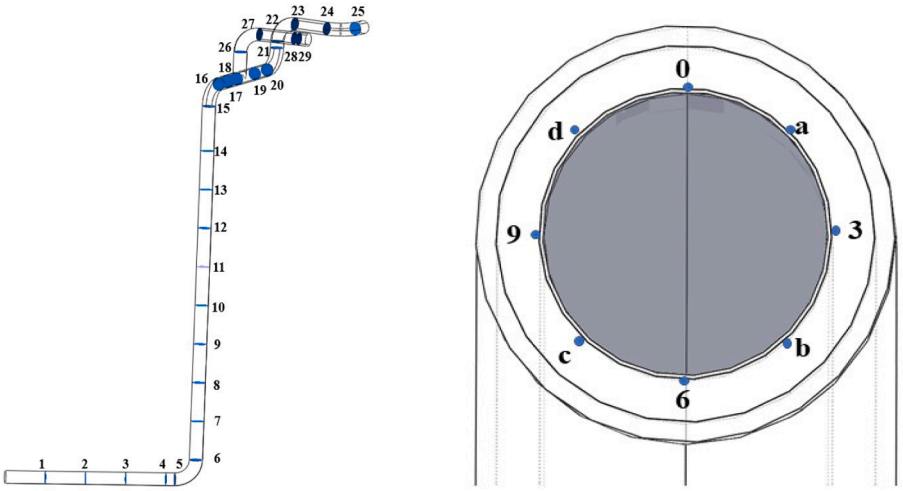
The pre-cooling and cold holding processes consist of seven stages, and the whole operation takes 23 hours. The pre-cooling stage lasts for 17 hours, while the cold holding continues 6 hours.

4.2.1. Pipe wall temperature distribution

As shown in Fig. 8, during the pre-cooling and cold holding, the pipe wall temperature distribution exhibits a similar pattern. During pre-cooling stages 1-3, the pipe temperature decreases slowly. Starting from pre-cooling stage 4, the temperature of the pipe wall decreases rapidly. This is caused by a significant decrease in the temperature of the incoming nitrogen.

The wall temperature distributions of the pipe in front of the tank, the riser, and the top section of the tank are plotted at the end of pre-cooling stage 4, as shown in Fig. 9. The circumferential temperature distribution is uneven, particularly in the horizontal pipe section before the tank and at the top of the tank. Additionally, the temperature at the top is significantly higher than at the bottom. In the elbow, the wall temperature decreases, and the circumferential temperature difference of the pipe wall reduces. After passing through the elbow, the riser exhibits a uniform circumferential temperature distribution, with the wall temperature gradually increasing along the flow direction. This phenomenon is mainly due to changes in the properties of the pre-cooled fluid and the influence of gravity, which causes fluid stratification. As a result, the heat transfer between the fluid and the upper and lower pipe walls becomes uneven. When the fluid passes through the elbow, disturbances disrupt the stratification, enhancing heat transfer between the fluid and pipe wall. The impact of gravity on fluid stratification in the riser is relatively small, leading to a reduced circumferential temperature difference in the riser pipe.

Temperature monitoring points at sections 2, 10, and 29 were selected for analysis, and the temporal evolution of temperature at these



(a) LNG feed line temperature monitoring surface

(b) Circumferential temperature monitoring points along the pipe wall

Fig. 7. Distribution of temperature monitoring points on LNG feed line.

locations is presented in Fig. 10. Section 2 exhibits the highest cooling rate due to its proximity to the inlet, where nitrogen first enters the pipeline with the largest temperature gradient and strongest convective potential, resulting in a rapid temperature decline. Section 10, located midstream, shows a moderate cooling rate, as the fluid has already absorbed heat upstream, reducing the temperature gradient. Moreover, the boundary layer at this location is more fully developed, which further diminishes convective heat transfer efficiency. In contrast, section 29, situated near the outlet, exhibits the slowest cooling rate. This is primarily due to the significantly lower temperature difference between the fluid and the pipe wall, as well as the potential presence of low-velocity zones, both of which reduce local convective heat transfer. By the end of the pre-cooling, the highest temperature is observed at the 0-point of section 25, reaching 205.2 K, while the lowest temperature appears at the 3-point of section 1, reaching 152.2 K. After the cold-holding, the highest temperature drops further to 176.29 K (0-point, section 25), and the lowest to 143.02 K (3-point, section 1). These results indicate that by the end of pre-cooling and cold-holding, the temperature throughout the entire pipeline system falls within the required operational range, thereby meeting the conditions for safe unloading.

During the pre-cooling and cold-holding stages, the temperature distribution along the circumferential direction of the pipe wall is notably non-uniform. The maximum temperature difference is observed at section 29, with a circumferential variation of up to 40 K and a radial variation of 23 K. Although the temperature difference between the top and bottom of the pipe remains below 50 K, which is within the acceptable range, prolonged exposure to a high temperature difference may cause damage to the pipeline.

The temperature drop rate of the feed pipeline, based on data from the monitoring points at sections 2, 10, and 29, is illustrated in Fig. 11. As a critical parameter during the pre-cooling, the temperature drop rate typically does not exceed 20 K/h. A comparison between the top and bottom of the pipe reveals that, at the onset of pre-cooling, the bottom exhibits a generally higher cooling rate with more pronounced fluctuations. Additionally, the temperature drop rate increases progressively closer to the pipe inlet. As pre-cooling progresses, the cooling rate at the bottom gradually decreases, while that at the top accelerates. This shift is attributed to the increasing temperature gradient between the upper pipe wall and the low-temperature fluid. As a result, during the later stages of pre-cooling and cold holding, the temperature drop rate at the top surpasses that at the bottom. The peak temperature drop rate occurs during the sixth stage of pre-cooling, when the inlet temperature decreases by 53 K compared to the previous stage. This causes a surge in the temperature drop rate at the bottom of the pipe in front of the tank, reaching 27 K/h.

During the pre-cooling, the temperature difference between the top and bottom of the pipeline initially increases, then gradually decreases as the stage progresses. This is due to the characteristics of the pre-cooling medium, where gravity causes the low-temperature medium in the horizontal pipe to first contact the bottom of the pipe, initiating heat transfer. As the fluid temperature rises, buoyancy causes the fluid to flow to the top of the pipe for further heat transfer. However, heat transfer at the top of the pipe is much smaller than at the bottom, resulting in a greater temperature drop at the bottom, thereby increasing the temperature difference between the top and bottom of the pipe. With the continuous injection of low-temperature media, the temperature at the bottom of the pipe decreases, reducing fluid heat transfer. Meanwhile, the temperature difference between the top of the pipe and the fluid increases, improving heat transfer. As a result, the temperature drop rate at the top increases, and the temperature difference between the top and bottom gradually reduces.

4.2.2. *The fluid temperature and flow state*

Low flow rates during the pre-cooling and cold-holding stages result in inadequate fluid movement within the pipeline, leading to a significant circumferential temperature difference at the top of the tank pipe. The fluid temperature at the upper inlet pipe monitoring points over time is shown in Fig. 12. During the pre-cooling and cold holding, the fluid temperature within the pipe exhibits uneven distribution along the circumference, with a maximum temperature difference of 48 K between the top and bottom of the pipe wall.

Fig. 13 presents the fluid temperature distribution in different pipeline segments at the end of pre-cooling stage 4. As pre-cooling progresses, the fluid gradually warms along the flow direction. Most of the fluid in the pipe section in front of the tank approaches the fluid inlet temperature. Upon entering the upper pipe section, the fluid temperature distribution becomes increasingly non-uniform. Stratification is observed in each horizontal segment, with the phenomenon particularly pronounced in the upper and lower inlet pipes.

Figs. 14 and 15 show the fluid temperature and density distributions at different monitoring sections at the end of pre-cooling stage 4. It is evident that the non-uniform distribution of fluid density within the

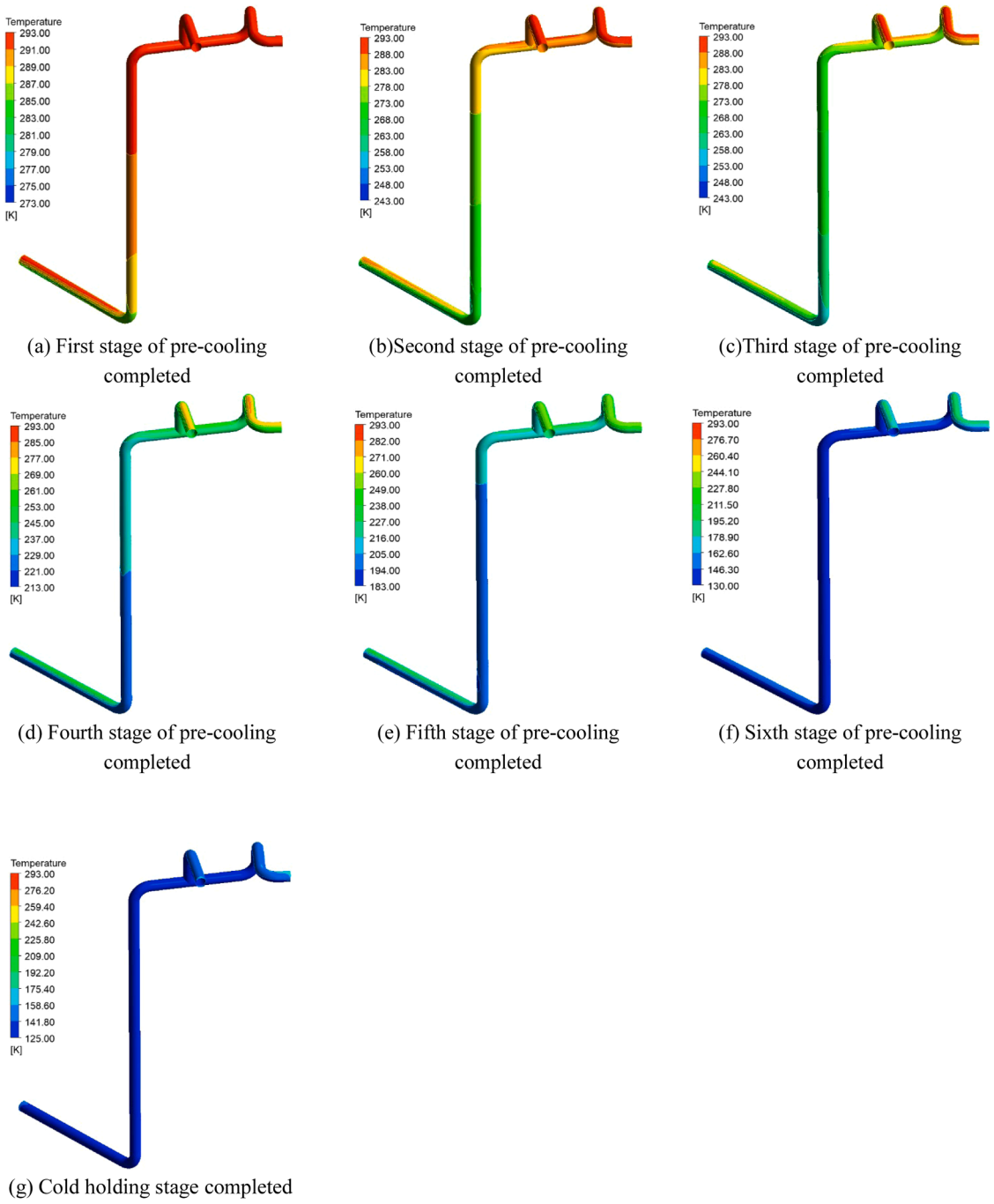


Fig. 8. Temperature distribution of the pipe wall at different stages.

pipeline is the primary cause of the temperature stratification. In the horizontal pipe segments (sections 2, 4, 24, 28), pronounced temperature stratification is observed, whereas in the vertical segment (sections 6, 10, 22, 26), the temperature field appears more uniform. This contrast results from the combined influence of gravity and buoyancy, which are governed by the temperature-dependent density variation of nitrogen gas. At lower temperature, the nitrogen becomes denser and is driven downward by gravity, leading to accumulation near the bottom of the pipe. Conversely, at higher temperature, nitrogen exhibits reduced density and is subject to upward buoyant forces. In horizontal sections, this stratification causes the cold nitrogen to concentrate near the pipe bottom, producing a larger thermal gradient and enhancing local convective heat transfer. Conversely, the upper region of the pipe, characterized by reduced fluid motion, exhibits lower heat transfer efficiency, resulting in considerable non-uniformity in thermal exchange. These opposing mechanisms result in a stable temperature stratification within the pipeline. Within the riser, the fluid flows in the direction of gravity, thereby suppressing stratification induced by density gradients and promoting a more homogeneous temperature field.

Fig. 16 presents the velocity field distributions at different monitoring sections.In straight pipe segments (sections 4, 10, and 28), the low flow velocity of nitrogen leads to weak momentum exchange, resulting in the absence of noticeable secondary vortical structures. At section 2, near the inlet, the incoming fluid exhibits an uneven velocity profile due to the lack of a fully developed boundary layer or axisymmetric flow. This condition gives rise to initial vortices or small-scale flow instabilities. Additionally, under less than full flow conditions, these vortices tend to be concentrated near the lower pipe. As the flow

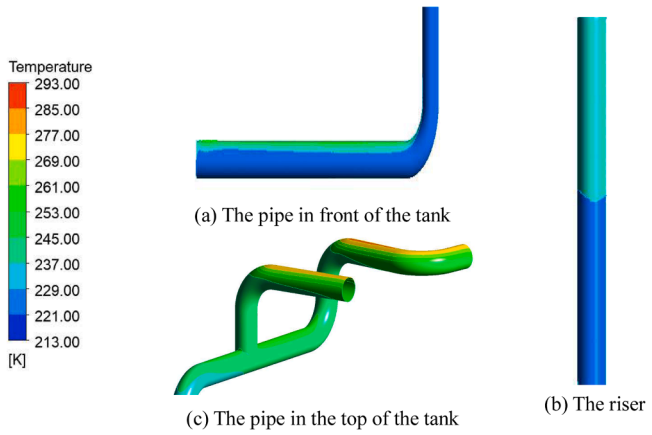


Fig. 9. Temperature distribution of pipe wall at the end of pre-cooling stage 4.

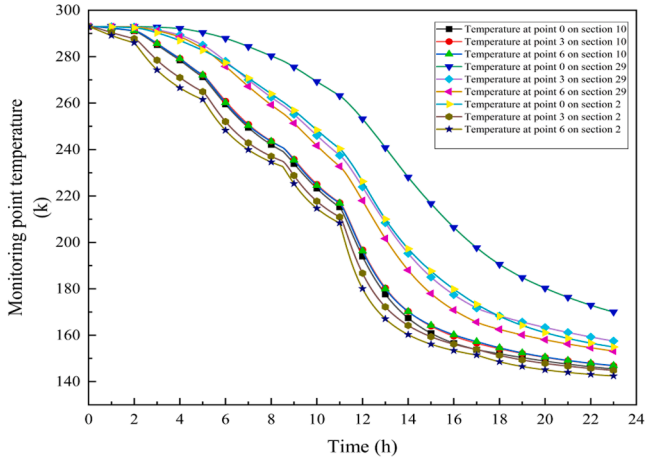


Fig. 10. Temperature variation curve of pipe wall monitoring points over time.

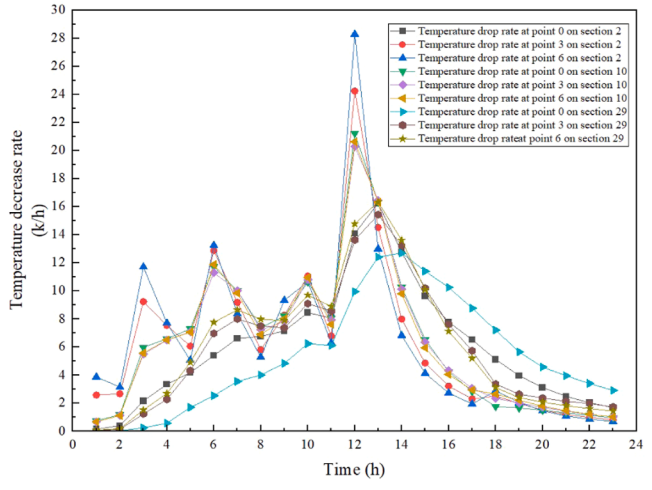


Fig. 11. Rate of the pipe wall temperature decrease.

continues downstream, such disturbances gradually decay, leading to the dissipation of vortical motion and thereby making straight horizontal sections more prone to thermal stratification.

In regions with abrupt changes in geometric curvature, such as near elbows and T-junctions (sections 6, 16, 20, 22, 24, and 26), prominent secondary vortex structures emerge. These vortices are primarily

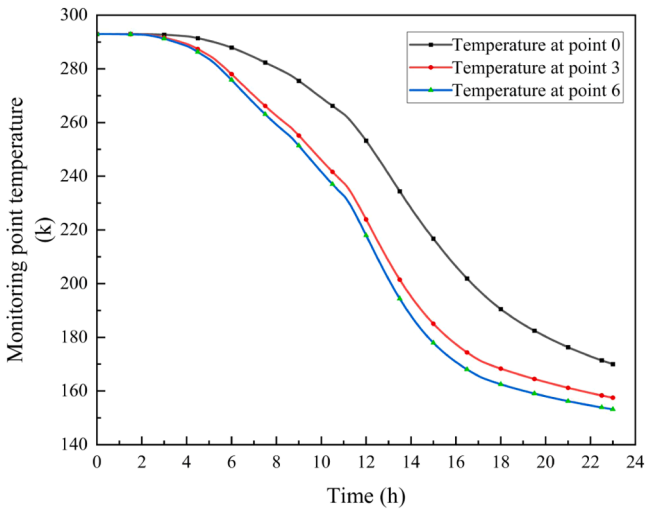


Fig. 12. Temperature variation curve on section 29 over time.

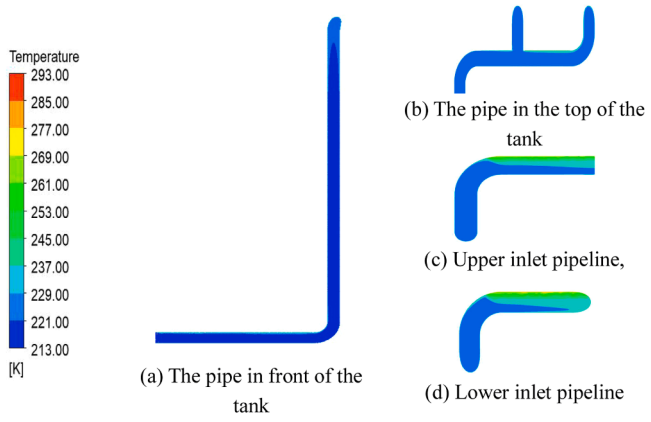


Fig. 13. Fluid temperature distribution at the end of pre-cooling stage 4.

induced by inertial centrifugal forces, flow redirection, and localized recirculation. The formation and evolution of these vortices are strongly governed by local pipe geometry and play a significant role in modulating convective heat transfer. Section 6 (immediately downstream of the first elbow) presents a classical Dean vortex structure characterized by a pair of symmetric, counter-rotating vortices with cores located near the pipe wall, driven by centrifugal forces. At section 16 (at the top of the riser near the tee), the secondary flow becomes asymmetric due to spatial torsion in the pipeline and the compounded influence of adjacent elbow and junction geometries, leading to an off-center vortex core. At section 20, shear-layer instabilities near the wall generate an eccentric single-vortex structure as a result of interfacial velocity gradients. The vortex structure further develops at section 22, where a well-defined pair of counter-rotating vortices forms, reflecting enhanced shear instability. After passing through the straight pipe segment, the upstream disturbances gradually decay, leading to a reduction in the strength of the counter-rotating vortices. As a result, the vortex structures become less pronounced at section 24. Finally, section 26, located within the vertical outlet branch, features a unidirectional recirculating vortex with its core displaced toward the branch wall, driven by low-velocity backflow associated with flow separation at the junction.

These observations confirm that inertial effects induced by geometric curvature dominate local flow dynamics and significantly influence thermal transport. Stronger vortices enhance fluid mixing, resulting in more uniform radial temperature fields. For example, sections 6, 16, 20, and 22 show vigorous secondary flows that disrupt thermal stratification

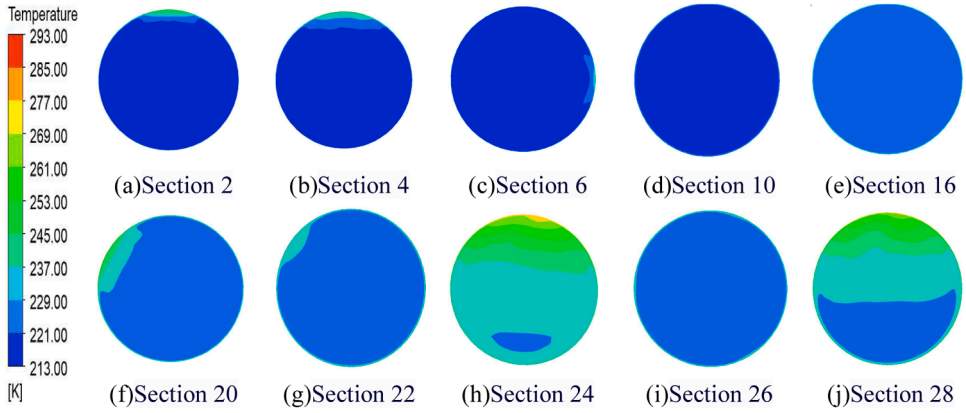


Fig. 14. Fluid temperature distribution at different sections at the end of pre-cooling stage 4.

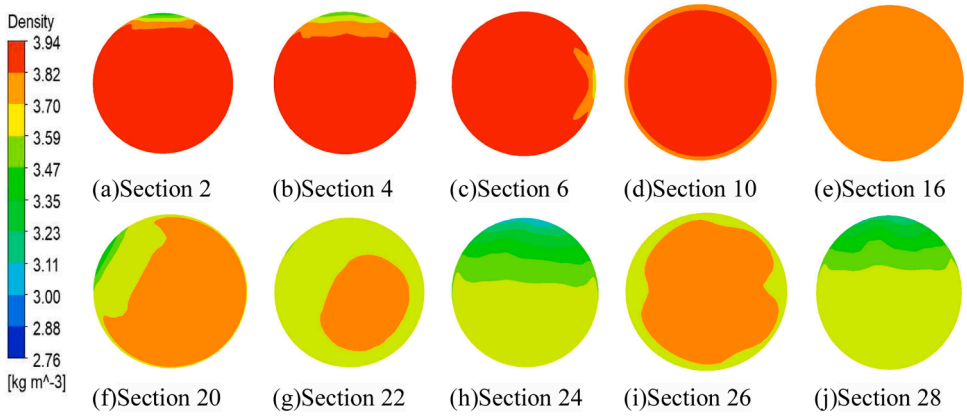


Fig. 15. Fluid density distribution at different sections at the end of pre-cooling stage 4.

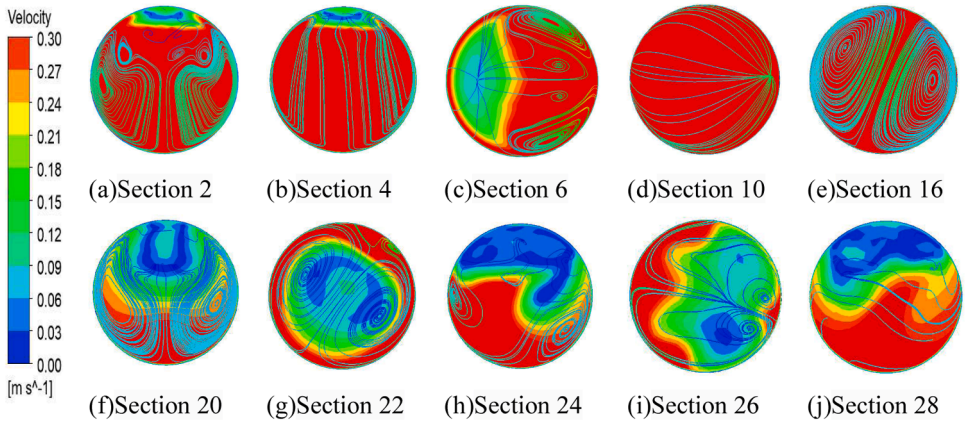


Fig. 16. Velocity and streamline distributions at different sections at the end of pre-cooling stage 4.

and promote convective heat transfer. In contrast, although section 24 is located near a bend, the weakened vortex activity allows stratification to persist, indicating limited thermal mixing. The presence of secondary flow disrupts and regenerates the boundary layer, increases radial velocity gradients, and promotes turbulent mixing and thermal diffusion. These findings underscore the critical role of geometric features—such as elbows and T-junctions—in shaping both flow structures and heat transfer performance, emphasizing their importance in the thermal design of pre-cooling pipelines.

4.3. Unloading

For unloading, the initial pipeline temperature is set to 183 K, the actual operating temperature of the pipeline at the LNG receiving terminal, analyzing the first 2 hours of results.

4.3.1. Pipe wall temperature distribution

Fig. 17 shows the pipe wall temperature distribution after 1 minute, 1 hour, and 2 hours under unloading condition. The wall temperature of the entire pipe system decreases rapidly as unloading progresses. After 1 minute of unloading, the temperature of the lower inlet pipe is higher

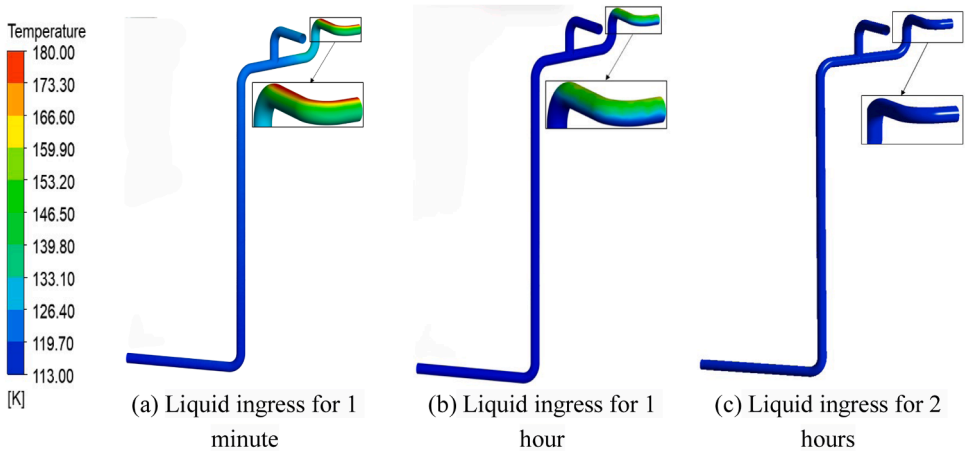


Fig. 17. Temperature distribution of pipe wall at different moments during unloading.

than that of the upper inlet pipe, and a noticeable temperature difference exists between the top and bottom of the lower inlet pipe. After 1 hour of unloading, the temperature of the upper inlet pipe approaches the fluid temperature, while the lower inlet pipe still shows uneven circumferential temperature distribution. After 2 hours of unloading, the temperature of the entire piping system decreases to a low and stabilized state.

The temperature of the pipe wall at monitoring points in different sections of 2, 10, 25, and 29 was selected and analyzed. As shown in Fig. 18, in the early stages of unloading, the pipe wall temperature decreases rapidly, with a temperature drop rate reaching up to 30 K/min. After approximately 20 minutes of unloading, the temperature throughout the pipeline, except for the lower feed pipe, drops to a low-temperature state. After 2 hours of unloading, the temperature of the entire pipe system stabilizes at approximately 130 K. The results show that, compared to the pre-cooling and cold holding, the temperature distribution along the pipe wall in the circumferential direction during the unloading process is more uniform. However, some temperature differences remain, with the largest difference of 31 K occurring between the top and bottom on section 25.

Fig. 19 shows the temperature change over time at the liquid and solid monitoring points in the upper inlet pipe. Due to the high flow rate of the unloading operation, LNG rapidly flows through the entire pipeline system. As the ultra-low temperature LNG contacts the pipeline, heat transfer occurs. However, thermal conduction through the wall thickness requires time, resulting in a significant temperature difference

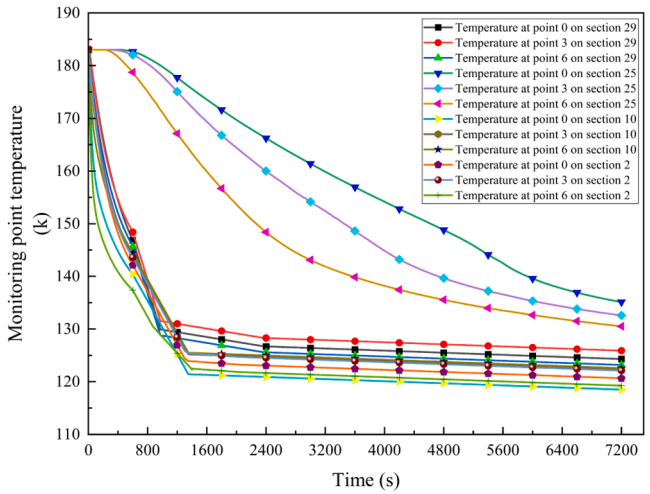


Fig. 18. Temperature variation curve of pipe wall monitoring points over time.

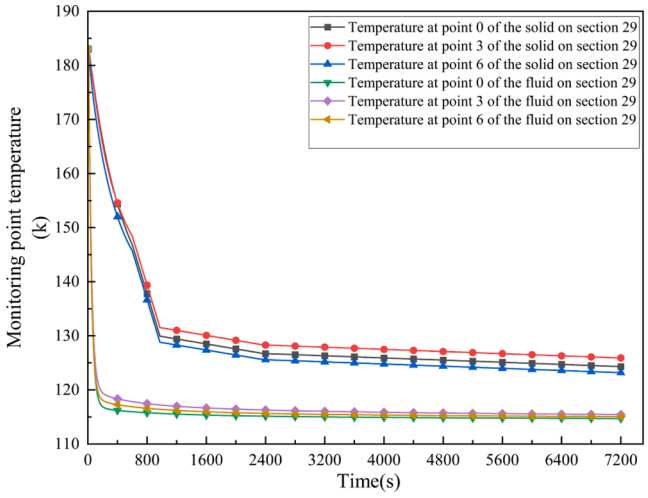


Fig. 19. Temperature variation curve on section 29 over time.

along the wall thickness, with the largest difference occurring at section 29, reaching a maximum of 53 K.

4.3.2. *The fluid temperature and flow state*

Fig. 20 presents the fluid temperature distribution across different pipeline segments 1 minute after the start of unloading. Figs. 21 and 22 show the fluid temperature and density distributions at different monitoring sections. At this point, except for the lower inlet pipe, the

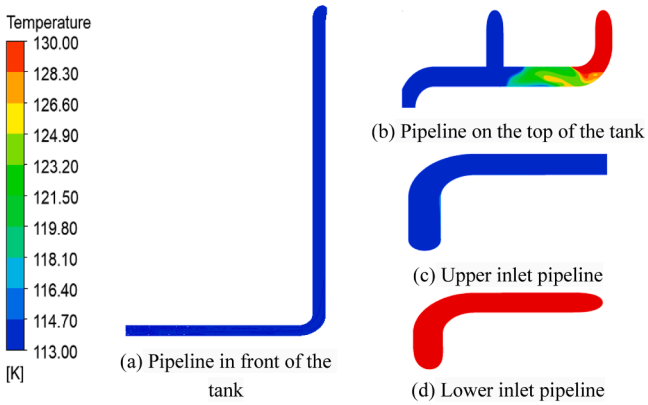


Fig. 20. Fluid temperature distribution at the end of 1 min unloading period.

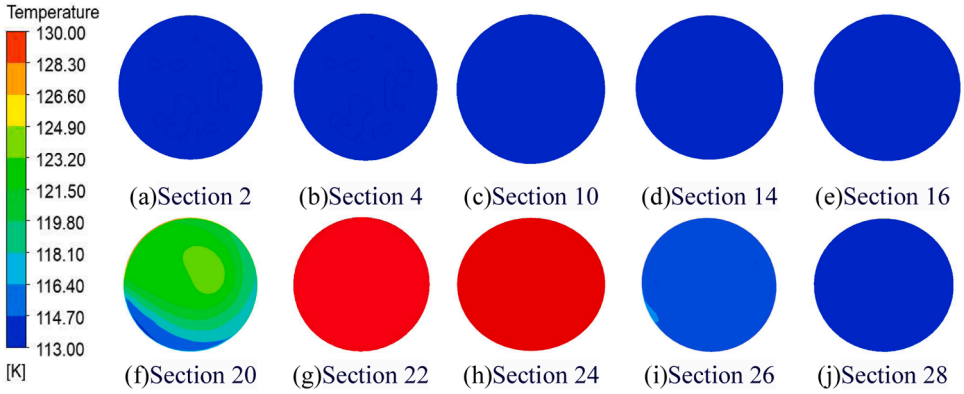


Fig. 21. Fluid temperature distribution at different sections at the end of 1 min unloading.

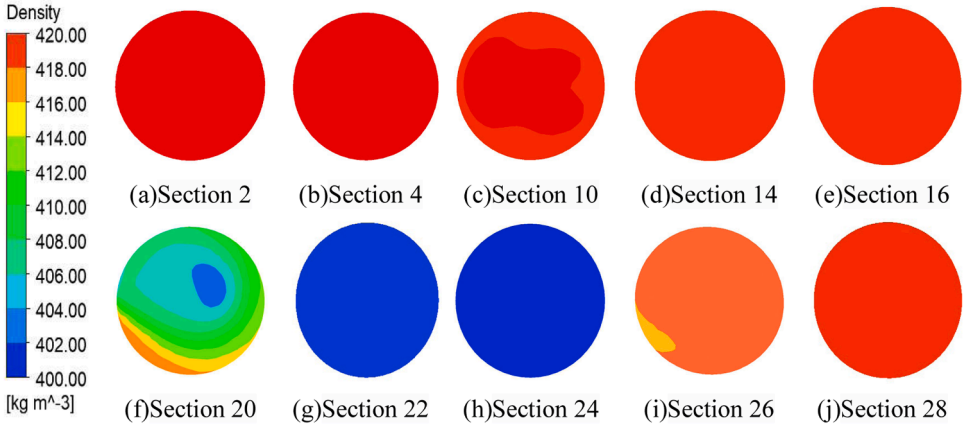


Fig. 22. Fluid density distribution at different sections at the end of 1 min unloading period.

fluid within the pipeline approaches full-flow conditions, with the internal temperature closely matching the inlet temperature. In contrast, the lower inlet pipe does not undergo unloading, with a small inflow and slow, uneven heat exchange between the liquid and pipe. As a result, the fluid temperature in the lower inlet pipe remains higher, with gravitationally induced temperature stratification clearly observed.

4.4. Parametric Analysis of Operating Conditions

During the operational phase of the pipeline, the predominant factors influencing temperature variation within the pipe include fluid flow rate, temperature, pressure, and the duration of the pre-cooling. As indicated in the previous analysis, the temperature evolution during the pre-cooling and cold holding exhibits similar patterns. In particular, the cold holding stage shows minimal temperature fluctuations, indicating a near-steady thermal state. In contrast, the unloading stage is characterized by a significantly higher flow rate, resulting in rapid temperature changes within the pipeline.

A parametric analysis is conducted in this section to investigate the pre-cooling and unloading processes. Based on the boundary conditions of the pre-cooling stage 1 and the unloading, a controlled-variable approach is employed. The analysis systematically varies the nitrogen flow rate and inlet temperature during pre-cooling, as well as the LNG flow rate during unloading, to investigate the thermal response of the pipeline under different operating conditions.

4.4.1. Analysis of pre-cooling parameter effects

As illustrated in Table 6, five operating conditions with different boundary settings were defined. Conditions 1 to 3 varied the inlet flow rate while maintaining constant inlet temperature and pressure, in order to investigate the effect of flow velocity on the thermal response of the pipeline. Conditions 1, 4, and 5 maintained a constant flow rate and pressure, with variations applied to the inlet temperature to investigate its impact on thermal behavior. The pre-cooling duration for all conditions was set to 2 hours.

Table 6
Boundary conditions of different pre-cooling cases.

Condition	Inlet temperature (K)	Inlet pressure (MPa)	Inlet flow rate (m/s)
1	273	0.15	0.1
2	273	0.15	0.215
3	273	0.15	0.36
4	263	0.15	0.1
5	253	0.15	0.1

Fig. 23 presents the temperature distribution along the pipe wall after 2 hours of pre-cooling under various operating conditions. As the nitrogen inlet flow rate increases and the inlet temperature decreases, the pipe wall temperature correspondingly declines. Nevertheless, a non-uniform circumferential temperature distribution remains pronounced in the horizontal pipeline. This phenomenon, consistent with previous observations, is primarily attributed to the combined influence of gravitational and buoyancy forces.

Figs. 24 and 25 depict the temporal evolution of the pipe wall temperature and the temperature difference between the top and bottom of the pipeline under various operating conditions, respectively. To investigate the spatial variation of the temperature field along the pipeline, sections 2, 10, and 29 were selected for detailed analysis.

As shown in Fig. 24, increasing the nitrogen flow rate or reducing its inlet temperature accelerates the rate of wall temperature decrease. The

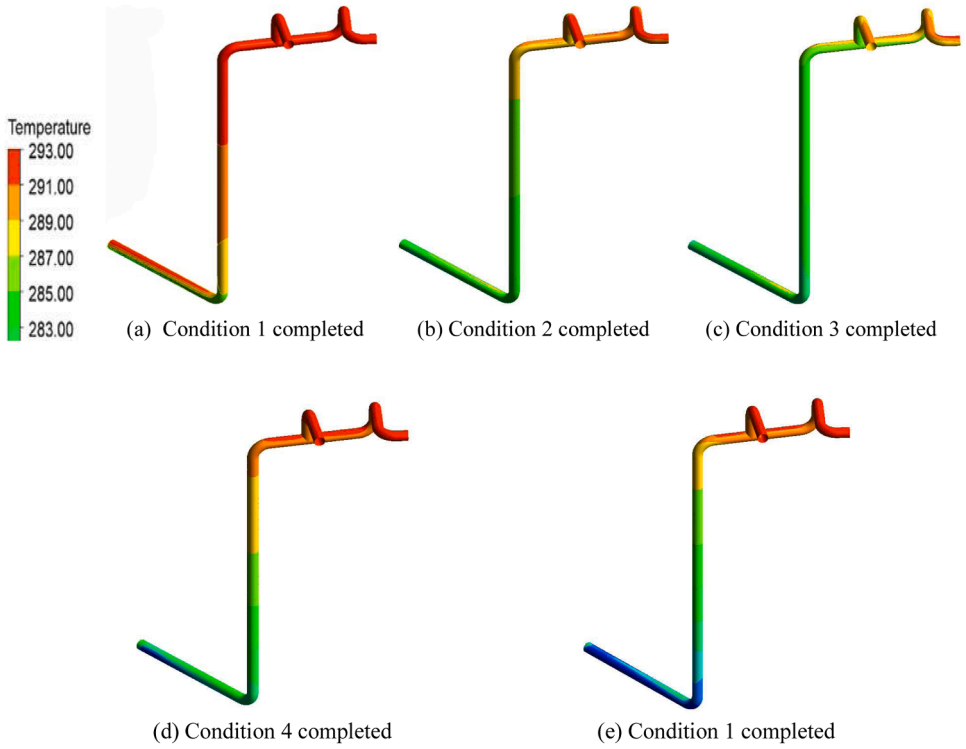
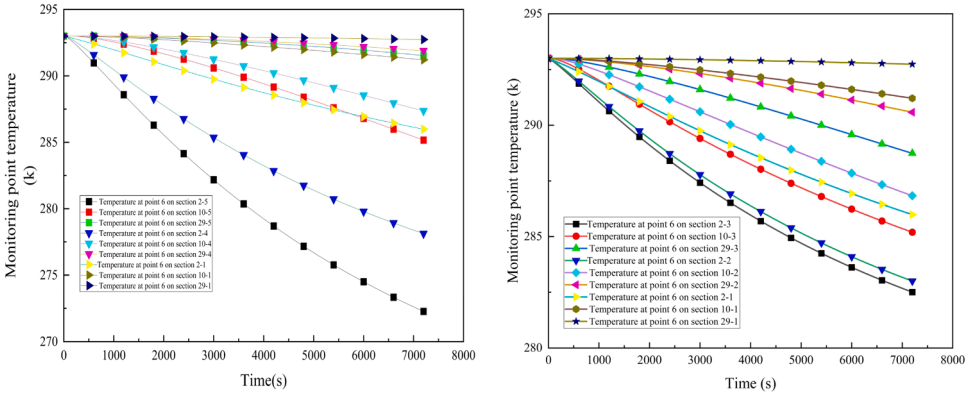
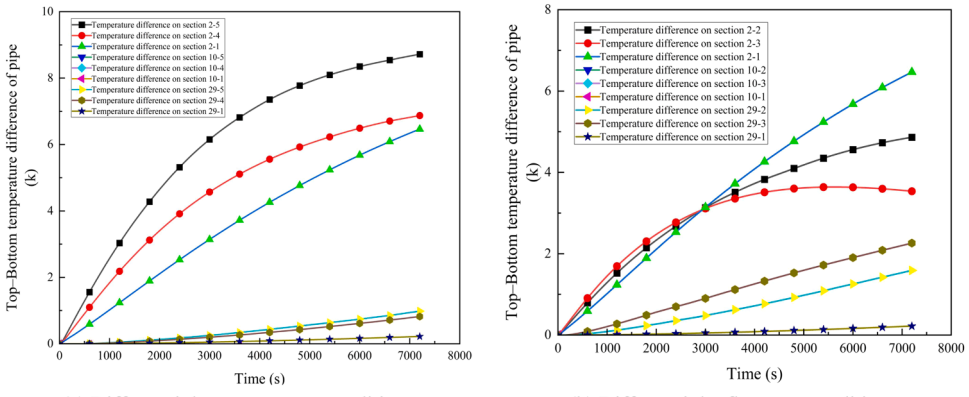


Fig. 23. Temperature distribution of the pipe wall after different pre-cooling conditions.



(a) Different inlet temperature conditions (b) Different inlet flow rate conditions

Fig. 24. Temperature variation at pipe wall under different conditions.



(a) Different inlet temperature conditions (b) Different inlet flow rate conditions

Fig. 25. Temperature difference between bottom and top of pipe wall under different conditions.

fastest temperature drop is observed when the inlet temperature is lowered to 253 K. Although a higher flow rate enhances the cooling effect, it is less effective than reducing the inlet temperature in improving overall cooling efficiency.

Fig. 25 further demonstrates that, when only the nitrogen inlet temperature is varied, lower temperatures result in a larger temperature difference between the top and bottom of the pipeline. This effect is particularly evident in the horizontal pipeline (sections 2 and 29), whereas the vertical pipeline (section 10) shows negligible top-to-bottom temperature difference. When only the nitrogen inlet flow rate is varied, the horizontal section near the inlet shows a non-monotonic trend in top-to-bottom temperature difference—initially increasing with flow rate and then decreasing. This behavior can be attributed to the interplay between flow dynamics and heat transfer mechanisms. At low flow rates, the flow is relatively slow and prone to partial flow conditions. During the early stage of pre-cooling, cold nitrogen tends to settle at the bottom of the pipe due to gravitational effects, leading to significant thermal stratification and thus a large top-to-bottom temperature difference. As the flow rate increases, enhanced flow disturbances promote better mixing and convective heat transfer, thereby mitigating the thermal stratification and reducing the temperature gradient. In contrast, in the vertical pipeline (section 10), where the flow direction is aligned with gravity, the influence of buoyancy is diminished. As a result, the nitrogen distribution becomes more uniform along the vertical axis, suppressing thermal stratification and resulting in an almost negligible top-bottom temperature difference. Furthermore, in the upper inlet pipe (section 29), a stable thermal field has not yet been fully established due to the limited pre-cooling duration. At higher flow rates, the contact time between the cold nitrogen and the pipe wall is reduced, and intensified flow disturbances lead to increased local thermal gradients. As a result, the top-to-bottom temperature difference becomes more pronounced with increasing flow rate.

4.4.2. *Analysis of unloading parameter effects*

As listed in Table 7, seven operating conditions were established, each with a different inlet flow rate. During the unloading process, the LNG introduced into the pipeline was maintained at a constant temperature. Consequently, the inlet temperature and pressure remained constant, while the inlet flow rate was varied to investigate its influence on the thermal response of the pipeline. According to previous studies, the temperature field evolves rapidly and tends to stabilize during unloading. Based on these findings, the simulation time for the unloading process was set to 30 minutes.

Fig. 26 shows the temperature variation of the upper inlet pipe wall over time under different unloading conditions. The results indicate that the unloading flow rate is positively correlated with the rate of temperature decrease. Fig. 27 illustrates the variation of the fluid–solid temperature difference across the wall thickness at the upper inlet pipe. A significant temperature difference develops in all cases, reaching a peak of approximately 55 K around 120 s after the start of unloading. This indicates a pronounced thermal imbalance between the fluid and the pipe wall during the initial stage. As time progresses, the temperature difference gradually decreases. Furthermore, it has been demonstrated that higher unloading flow rates result in a more rapid decline in temperature difference, which can be ascribed to enhanced convective heat transfer. Increased flow velocity promotes more efficient thermal exchange, thereby accelerating the homogenization of temperature across the wall thickness.

Table 7
Boundary conditions of different unloading cases.

Condition	Inlet temperature (K)	Inlet pressure (MPa)	Inlet flow rate (m/s)
1	115	0.158	3
2	115	0.158	3.5
3	115	0.158	4
4	115	0.158	4.5
5	115	0.158	5
6	115	0.158	5.5
7	115	0.158	6

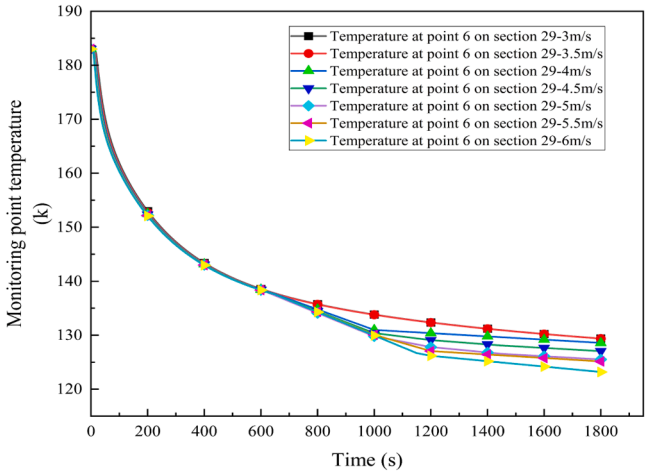


Fig. 26. Temperature variation curve on section 29 with time at different unloading speeds.

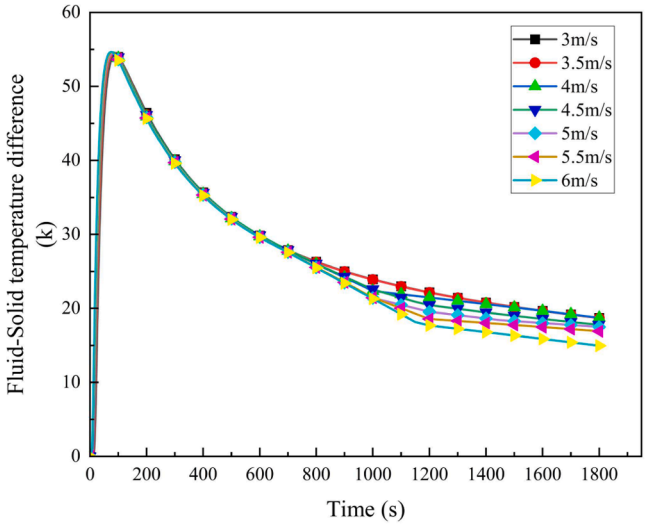


Fig. 27. Fluid-Solid temperature difference under different unloading flow rates.

4.5. *Heat Transfer Mechanisms Under Varying Operating Conditions*

Based on the simulation results, the heat transfer performance of the feed pipeline is analyzed during the pre-cooling, cold holding, and unloading stages. The average Nusselt number at the pipe wall for each stage is calculated using Eq. (1). At the end of each stage, the characteristic length is defined as $l = 0.9896$ m, and the inlet fluid temperature at the beginning of the stage is used as the reference temperature for calculating the heat transfer coefficient. The average Nusselt number is then obtained in Fluent using the area-weighted average method. Table 8 presents the variations in the Nusselt number and the Turbulent Kinetic Energy (TKE) across different stages. Stages 1-6 correspond to six consecutive pre-cooling stages, stage 7 to cold holding, and stage 8 to unloading. The Nusselt number increases progressively during pre-cooling, indicating enhanced convective heat transfer efficiency between the fluid and the pipe wall. In particular, in the sixth stage of pre-cooling, the Nusselt number increases by 63.9% compared to the previous stage. This significant change is primarily attributed to the lower

Table 8
Turbulent kinetic energy and Nusselt number under different stages.

Stage	Turbulent kinetic energy (m^2/s^2)	Nusselt number
1	0.0016	52.33
2	0.0047	132.58
3	0.0056	190.36
4	0.0050	231.54
5	0.0058	260.26
6	0.0042	426.55
7	0.0018	261.69
8	0.1383	33,072.53

fluid temperature relative to the pipe wall, which leads to a considerable increase in the convective heat transfer rate. During the unloading process, the high flow rate and ultra-low temperature of LNG induce strong turbulence, leading to a large temperature difference between the fluid and the pipe wall. As a result, convective heat transfer is significantly enhanced. The Nusselt number in this stage is substantially higher than that in the pre-cooling and cold holding stages, causing the pipeline temperature to quickly drop to a low and stable state.

The TKE exhibits a non-monotonic trend across different stages. Specifically, the TKE is relatively low during the pre-cooling stage 1. Although minor fluctuations occur during stages 2 to 5, the overall trend is upward. During pre-cooling stage 6 and the cold holding, the TKE gradually decreases, followed by a sharp increase during the unloading. In contrast, the Nusselt number increases continuously throughout the entire process.This divergence can be explained from the perspectives of flow dynamics and heat transfer mechanisms. The TKE reflects the intensity of turbulence within the fluid and is influenced by physical properties such as flow velocity, density, and viscosity. The flow velocity in stages 2 to 5 is significantly higher than in stage 1, resulting in substantially greater TKE during these stages. Although the flow velocity remains constant from stages 3 to 6, the inlet temperature continuously decreases. As a result, the viscosity of nitrogen gas decreases while its density increases. These changes lead to steeper viscosity gradients and a thinner boundary layer, which may locally suppress turbulence generation and cause the observed non-monotonic variations in TKE.On the other hand, the Nusselt number is primarily governed by the temperature difference between the fluid and the pipe wall. Despite fluctuations in TKE, the continuous decline in fluid temperature during pre-cooling leads to an increasing temperature gradient across the pipe wall. This enhances the thermal driving force, thereby improving the overall convective heat transfer efficiency and resulting in a sustained rise in the Nusselt number.

Fig. 28 illustrates the distribution of vorticity within the feed pipeline at different stages. Subfigures (a)–(f) correspond to stages 1 to 6 of the pre-cooling stage, (g) represents the cold holding stage, and (h) corresponds to the unloading stage. The vorticity characterizes the strength of rotational motion in the fluid and is closely related to flow field disturbances. It can be observed that the vorticity in pre-cooling stage 6 is significantly higher than in the other pre-cooling and cold holding stages, while the vorticity during unloading is markedly higher than in both the pre-cooling and cold holding stages. When comparing these results with the Nusselt number and TKE, it becomes evident that higher vorticity corresponds to more intense vortex motion within the fluid. This intensified vortex activity disrupts the thermal boundary layer and reduces thermal resistance, thereby enhancing convective heat transfer. Moreover, increased vorticity promotes stronger velocity fluctuations and greater turbulence intensity, which further contributes to the rise in TKE. It is also noteworthy that vorticity increases significantly when the fluid passes through bends, T-junctions, and other complex pipeline structures. This is primarily because such configurations alter the flow path and direction. Due to centrifugal effects, the fluid on the outer side of a bend moves faster and experiences lower pressure, while the inner side exhibits slower velocity and higher pressure. This pressure differential induces lateral flow within the fluid, leading to the formation of vortices. These vortices disrupt the boundary layer, thereby improving the convective heat transfer performance.

Table 9 and 10 present the variations in Nusselt number and TKE under different working conditions during the pre-cooling and unloading stages, respectively. As shown in Table 9, during the pre-cooling

Table 9
Turbulent kinetic energy and Nusselt number under different pre-cooling conditions.

Condition	Turbulent kinetic energy (m^2/s^2)	Nusselt number
1	0.0016	52.33
2	0.0028	105.35
3	0.0035	142.12
4	0.0022	72.33
5	0.0026	79.82

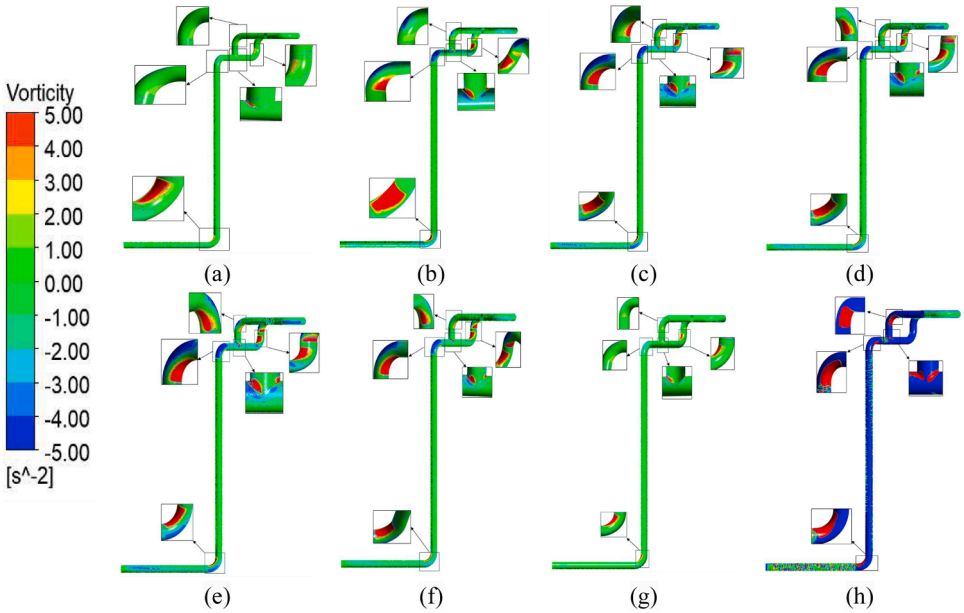


Fig. 28. Vorticity distribution within the pipe during different operational phases.

Table 10
Turbulent kinetic energy and Nusselt number under different unloading conditions.

Condition	Turbulent kinetic energy (m^2/s^2)	Nusselt number
1	0.0659	24,207.62
2	0.0872	27,409.09
3	0.1163	30,411.05
4	0.1383	33,072.53
5	0.1632	37,350.21
6	0.1865	39,271.76
7	0.2178	43,090.39

process, both the Nusselt number and TKE increase with rising flow rates and decreasing inlet temperatures. It is noteworthy that although conditions 2 and 3 exhibit higher Nusselt numbers and TKE values than conditions 4 and 5, the wall temperature in condition 5 decreases at the fastest rate. This phenomenon can be attributed to the fact that the flow velocities in conditions 2 and 3 are approximately 115% and 260% higher, respectively, than those in conditions 4 and 5. Since both the convective heat transfer coefficient and TKE are strongly influenced by flow velocity, the Nusselt numbers in conditions 2 and 3 are significantly higher. However, the lower inlet temperatures in conditions 4 and 5 lead to larger temperature differences between the fluid and the pipe wall. Although the temperature difference does not directly affect the convective heat transfer coefficient, it has a direct impact on the amount of heat transfer. As a result, the greater thermal gradient in conditions 4 and 5 enhances the heat flux, leading to a faster reduction in the pipe wall temperature despite the relatively lower Nusselt numbers.

As shown in Table 10, both the Nusselt number and TKE increase consistently with rising unloading flow rate. This trend can be attributed to the fact that higher flow velocities intensify fluid disturbances and accelerate the renewal of the thermal boundary layer, thereby significantly enhancing convective heat transfer efficiency. The increased heat transfer efficiency leads to a rapid reduction in the temperature difference between the fluid and the pipe wall, while also flattening the temperature gradient across the pipe wall thickness. Consequently, the homogenization of the pipe wall temperature field is accelerated, and the thermal field within the pipeline tends to stabilize within a relatively short period during the unloading process.

The results demonstrate that both the Nusselt number and TKE are strongly influenced by flow rate and fluid temperature across different operational stages. During the pre-cooling process, the gradual increase in flow velocity and decrease in inlet temperature lead to enhanced convective heat transfer, as evidenced by the continuous rise in the Nusselt number. Despite non-monotonic variation in TKE, the overall heat transfer efficiency improves due to increasing thermal gradient between the fluid and the pipe wall. The unloading stage exhibits the highest levels of vorticity, TKE, and Nusselt number, resulting in rapid thermal homogenization of the pipeline. Vorticity analysis further confirms that complex geometries, such as bends and T-junctions, intensify turbulence and promote boundary layer disruption, thereby contributing to improved heat transfer performance. These findings highlight the critical roles of flow dynamics and fluid properties in optimizing thermal management in cryogenic pipeline systems.

5. Conclusion

In this study, a numerical simulation method is employed to investigate the heat transfer characteristics of LNG pipelines. First, the applicability and accuracy of the RANS method for solving the fluid-solid heat coupling problems are validated using a benchmark model. Based on specific assumptions, the feeding operation of an LNG receiving station is simplified, and a numerical simulation model is developed to thoroughly analyze the flow behavior and heat transfer mechanisms during the pre-cooling stage, cold holding, and unloading process. Furthermore, different operating conditions are investigated to elucidate the effects of key parameters, such as flow rate and temperature, on the heat transfer performance and flow characteristics. The simulation results reveal critical issues such as flow maldistribution, temperature stratification, and differences in heat transfer efficiency within the pipeline. These findings provide theoretical support for the optimized design and operation of LNG pipeline systems and offer a practical reference for future engineering applications. The main conclusions are as follows:

(1) The temperature field distribution of the LNG feed pipeline exhibits a similar pattern during both the pre-cooling and cold holding stages. Significant flow maldistribution occurs within the pipeline, resulting in pronounced temperature stratification in the horizontal section upstream of the tank and at the tank top. This results in inconsistent temperature drop rates along the pipeline, with the maximum rate reaching up to 27 K/h. In addition, substantial circumferential non-uniformity in the wall temperature distribution is observed, particularly at the top and bottom of both the upper and lower feed pipelines, where the maximum temperature difference can reach 40 K. This indicates that the temperature field in the feed pipeline is highly non-uniform under pre-cooling and cold holding conditions. To mitigate the excessive circumferential thermal gradients and improve the uniformity of the wall temperature distribution, low-temperature spray cooling or similar local enhancement techniques could be considered for the upper and lower feed pipelines.

(2) During the LNG unloading process, the temperature of the whole pipe system will drop rapidly, with the temperature decrease rate can be up to 30 K/min, and the flow state in the pipe is close to full flow. The unloading process is characterized by a high flow rate and ultra-low temperature, which leads to a very small difference in temperature distribution along the pipe wall in the circumferential direction, but there is a large temperature difference along the wall thickness direction, especially in the upper inlet pipe, where the difference reaches 53 K.

(3) Cold holding temperature is a crucial factor for the structural safety of the LNG feed pipeline. Excessive cold holding temperature may cause the pipeline's stress to exceed the material's yield strength, resulting in the risk of crack failure. In actual production, the pipeline cooling temperature should be strictly controlled, with pre-cooling and cold holding lasting 23 hours. Temperature monitoring should also be conducted as needed to monitor the flow behavior of the medium within the pipeline.

(4) The flow rate and temperature of the fluid medium are the primary factors influencing variations in heat transfer efficiency within the LNG feed pipeline. During the pre-cooling stage, the inlet temperature exerts a more pronounced impact on the evolution of pipeline wall temperature than the inlet flow rate. Accordingly, pre-cooling efficiency can be enhanced by appropriately increasing the inlet flow rate or decreasing the inlet temperature. The heat transfer efficiency of the LNG feed pipeline during the unloading stage is significantly higher than that during the pre-cooling and cold holding stages. Although heat transfer efficiency varies with different unloading rates, its effect on fluctuations in pipeline wall temperature remains relatively limited.

(5) Complex pipeline structures, such as elbows and T-junctions, play a critical role in shaping local flow patterns and influencing convective heat transfer, making them key design considerations in the thermal management of cryogenic pipeline systems. This effect is primarily attributed to the abrupt changes in curvature and flow direction caused by these structures, which generate secondary vortices and associated flow disturbances. These phenomena enhance turbulence intensity and disrupt the thermal boundary layer, thereby promoting fluid mixing and increasing radial temperature gradients, which together contribute to improved convective heat transfer efficiency in critical pipeline regions.

CRediT authorship contribution statement

Hongyu Zhou: Writing – original draft, Validation, Software, Data

curation. **Xu Sun:** Writing – original draft, Methodology, Investigation. **Tao Di:** Validation, Software, Methodology. **Xiaoben Liu:** Writing – review & editing, Data curation. **Hong Zhang:** Writing – review & editing.

Declaration of competing interest

The authors declare that they have no known competing financial interests or personal relationships that could have appeared to influence the work reported in this paper.

References

Castillo, L., Dorao, C.A., 2013. On the conceptual design of pre-cooling stage of LNG plants using propane or an ethane/propane mixture. Energy Convers. Manag. 65, 140–146.

Darr, S.R., Hartwig, J.W., 2020. Two-phase convection heat transfer correlations for liquid hydrogen pipe chilldown. Cryogenics 105, 102999.

De, S., Fu, Z., Che, J., et al., 2013. Numerical Simulation of Liquefied Natural Gas in Rib-Tube. Appl. Mech. Mater. 483, 162–165.

Golda, P., Schießl, R., Stampfer, B., et al., 2021. Experimental determination of the cooling performance of liquid nitrogen for machining conditions. Int. J. Heat Mass Transf. 164, 120588.

He, T.B., Ju, Y.L., 2014. Performance improvement of nitrogen expansion liquefaction process for small-scale LNG plant. Cryogenics 61, 111–119.

Hu, H., Chung, J.N., Amber, S.H., 2012. An experimental study on flow patterns and heat transfer characteristics during cryogenic chilldown in a vertical pipe. Cryogenics 52 (4–6), 268–277.

Jin, L., Cho, H., Lee, C., et al., 2018. Experimental research and numerical simulation on cryogenic line chill-down process. Cryogenics 89, 42–52.

Jin, L., Park, C., Cho, H., et al., 2016. Experimental investigation on chill-down process of cryogenic flow line. Cryogenics 79, 96–105.

Johnson, J., Shine, S.R., 2015. Transient cryogenic chill down process in horizontal and inclined pipes. Cryogenics 71, 7–17.

Kunniyoor, K.R., Govind, R., Venkateswaran, K.S., et al., 2021. Liquid hydrogen pipeline chill-down: mathematical modelling and investigation. Cryogenics 118, 103324.

Kuroki, T., Sakoda, N., Shinzato, K., et al., 2018. Prediction of transient temperature of hydrogen flowing from pre-cooler of refueling station to inlet of vehicle tank. Int. J. Hydrog. Energy 43 (3), 1846–1854.

Li, J., Gong, Z., Ma, H., et al., 2024. Numerical simulation and thermal analysis of water circulation cooling pipe of pressurized hydrogen ship-board cylinders. Case Stud. Therm. Eng. 59, 104534.

Liao, J., Yuan, K., Mei, R., et al., 2005. Cryogenic chilldown model for stratified flow inside a pipe.

Liao, J., Mei, R., Klausner, J.F., 2006. A film boiling model for cryogenic chilldown at low mass flux inside a horizontal pipeline. Heat Mass Transf. 42 (10), 891–900.

Lim, C.L., Adam, N.M., Ahmad, K.A., 2018. Cryogenic pipe flow simulation for liquid nitrogen with vacuum insulated pipe (VIP) and Polyurethane (PU) foam insulation under steady-state conditions. Therm. Sci. Eng. Prog. 7, 302–310.

Liu, L., Guo, T., Kong, X., et al., 2024a. Design and optimization of liquid nitrogen precooling BOG re-liquefaction process for LNG ships. Int. J. Refrig. 159, 134–146.

Liu, X., Zhao, Z., Li, C., et al., 2024b. Investigation of local flow and heat transfer of supercritical LNG in airfoil channels with different vortex generators using field synergy principle. Appl. Therm. Eng. 242, 122424.

Qyyum, M.A., Qadeer, K., Ahmad, A., et al., 2020. Two-phase expander refrigeration cycles with ethane–nitrogen: a cost-efficient alternative LNG processes for offshore applications. J. Clean Prod. 248, 119189.

Shaeffer, R., Hu, H., Chung, J.N, 2013. An experimental study on liquid nitrogen pipe chilldown and heat transfer with pulse flows. Int. J. Heat Mass Transf. 67, 955–966.

Shukri, T., 2004. LNG technology selection. Hydrocarb. Eng. 9, 71–76.

Soujoudi, R., Manteufel, R., 2023. Thermodynamic advantages of flash intercooling in natural gas liquefaction's precooling cycle. Energy Rep. 10, 793–804.

Véchot, L., Olewski, T., Osorio, C., et al., 2013. Laboratory scale analysis of the influence of different heat transfer mechanisms on liquid nitrogen vaporization rate. J. Loss Prev. Process. Indust. 26 (3), 398–409.

Venkatesh, N., Kumar Agarwal, D., Salih, A., et al., 2023. Chilldown of cryogenic feed lines- An insight into the influence of feed line orientation and mass flux. Cryogenics 130, 103644.

Wang, Y., Wang, F., Zheng, W., et al., 2023. Experimental study of flow distribution behavior on the shell side of spiral tube bundles in LNG spiral-wound heat exchangers. Therm. Sci. Eng. Prog. 45, 102106.

Wu, C., Liu, J., Zhang, J., 2024. Transient thermal analysis on pre-cooling process of LNG cryogenic corrugated hose. Geoenergy. Sci. Eng. 232, 212434.

Yuan, K., Ji, Y., Chung, J.N., 2007. Cryogenic chilldown process under low flow rates. Int. J. Heat Mass Transf. 50 (19–20), 4011–4022.

Yuan, K., Ji, Y., Chung, J.N., 2009. Numerical modeling of cryogenic chilldown process in terrestrial gravity and microgravity. Int. J. Heat Fluid Flow 30 (1), 44–53.

Zhang, P., Fu, X., 2009. Two-phase flow characteristics of liquid nitrogen in vertically upward 0.5 and 1.0mm micro-tubes: visualization studies. Cryogenics 49 (10), 565–575.

Zhu, J., Zheng, B., Wang, S., et al., 2023. Boil-off gas precooling process for subsea low temperature LNG pipelines. Sustain. Horiz. 8, 100070.